Scholars Bulletin *(Engineering and Technology)*

An Official Publication of "Scholars Middle East Publishers", Dubai, United Arab Emirates
Website: http://scholarsbulletin.com/

ISSN 2412-9771 (Print)
ISSN 2412-897X (Online)

Numerical Study of the Physical Properties of InGaN Lasers for 1.55 μm Applications

Md. Jahirul Islam[1*], Md. Rafiqul Islam[1]

[1]Department of Electrical and Electronic Engineering, Khulna University of Engineering & Technology, Khulna-9203, Bangladesh

***Corresponding author**
Md. Jahirul Islam

Article History
Received: 15.09.2017
Accepted: 20.09.2017
Published: 30.09.2017

DOI:
10.21276/sb.2017.3.9.4

Abstract: In this paper, we investigate the bandgap energy, lattice constants, optical confinement factor, and physical properties of InGaN based quantum well lasers for 1.55 μm applications. Linear interpolation between the experimentally determined values of InN and GaN is used to calculate the lattice constants and the composition of the composite InGaN for the desired bandgap energy. Solving the Schrödinger equation in conjunction with k.p method and Luttinger-Kohn Hamiltonian matrix operator, the band profiles are calculated for the quantum well structure. First, the probability distribution is calculated, later which describes the electron density in the quantum well, and a value of 10^{-18} cm^{-3} is found from the calculations. In addition, the energies of conduction and valence bands are clearly demonstrated, and the corresponding heavy and light holes states are examined clearly. Determination of these parameters is of immense important for the microstructural fabrication, laser pumping power requirements, and practical applicability of the proposed laser structure.

Keywords: Heterostructure, InGaN laser, Quantum well laser, Physical properties

INTRODUCTION

The long-distance, high-speed, and extremely bulky data-rate transmission is of immense important for the modern ages [1]. The 1.55 μm wavelength is the best suited window for long distance fiber optic communication system compared to 1.3 μm and 0.85 μm windows. At 1.55 μm wavelength the attenuation and transmission losses are very low, and thus made it an excellent candidate for future all-optical communication infrastructure [2-3].

Recently, semiconductor based lasers have been focused in the application of optical systems as the light sources [4-5]. A number of researchers demonstrated many semiconductor structures for lasing purposes. This includes vertical cavity surface emitting lasers (VCSEL), buried heterostucture lasers, quantum well lasers, and quantum dot lasers [6-9].

To get 1.55 μm laser output, a bandgap energy of 0.8 eV is required. The present active layer materials of the lasers consist of ternary, quaternary and quintuplet materials such as InGaAs/InGaAsP, AlGaInAs, GaInNAsSb/GaAs and GaInNAsSb/ GaNAs [10-13]. Due to fabrication challenge and associated complexity, these materials may produce lasing problem. Moreover, the InGaAs/InGaAsP system has the disadvantage that the discontinuity in valence band ΔE_v, is much larger than the discontinuity in conduction band ΔE_c, and thus, preventing a strong localization of the electrons [14].

The GaN semiconductor materials composited with proper In fraction results in $In_xGa_{1-x}N$ alloys which necessarily can emit lights of 1.55 μm. The InGaN material is believed to be a promising candidate for future 1.55 μm laser sources [4]. However, the demonstration of the InGaN based lasers and their practical applicability are in infancy till now. Therefore, further studies on the physical properties and performance characterization are required.

In this paper, we investigate the physical properties of InGaN materials in a quantum well (QW) structure for 1.55 μm laser applications. The bandgap energy, lattice constants, and both the valence and conduction band profiles are investigated thoroughly. In the analysis, the probability distribution and electron density in different bands are discussed briefly. It is noted that all the simulation works are carried out using Matlab.

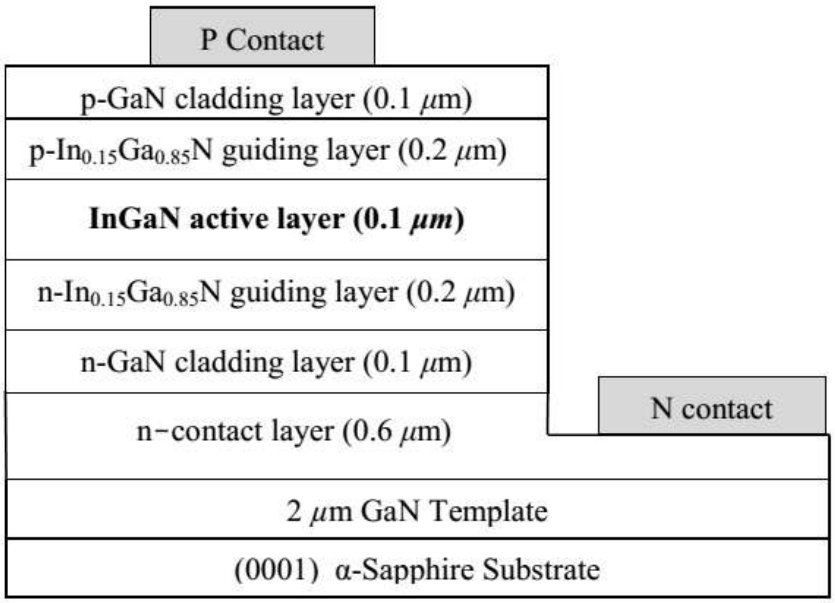

Fig-1: Schematic structure of the proposed edge emitting QW laser (After Ref. [15].

Proposed Physical Model of Laser

The laser device comprising a hetero structure that is composed of an active layer, and a pair of cladding layers which sandwiches the active layers in between. The optical guiding layers are positioned between one cladding layer and the active layer and between the active layer and the other cladding layer. A striped contact layer in which current injected into the laser device is confined. The schematic structure of the proposed 1.55 μm quantum-well heterostrucre lasers using InGaN is shown in Fig. 1. A c-plane sapphire wafer is used as the substrate. The laser structure consists of 0.6 μm thick nickel as n-contact and gold as p-contact, 0.1 μm thick GaN cladding layer, 0.2 μm thick $In_{0.15}Ga_{0.85}N$ guiding layer, and a 0.1 μm thick InGaN active layer along with 0.1 μm thick $In_{0.15}Ga_{0.85}N$ barrier layer. The guiding layers termed as index guiding waveguides are used in laser to confine the laser light in active region. The cladding layers are used to reduce the penetration of the optical mode outside the guiding layers [16]. It facilitates to activate the leakage current due to drift and diffusion of electrons through the p-cladding layer. It is worth noting that the leakage current increases as the cladding thickness is reduced [17].

Simulation Process

Simulation and characterization on InGaN based lasers are very immature. To realize a physical structure, simulations on structure and parameter optimization are necessary. This section describes the simulation processes adopted to analyze the physical properties of the proposed laser model. This includes the band gap energy determination, composition of constituent materials, lattice constants, and electronic band energy calculation for both conduction and valence bands.

Composition of In and Ga

In recent years most of the intensive research has been focused on Ga-rich $In_xGa_{1-x}N$ and $Ga_xAl_{1-x}N$ alloys whose energy gaps cover the short wavelength-visible and near ultraviolet parts of the electromagnetic spectrum [17]. It was suggested that the band gap of InN should be much smaller than 1.9 eV [18]. Recently new band gap of 0.65 eV for InN has been reported [18-19]. The band gap of the ternary alloy $In_xGa_{1-x}N$ can be approximated by the parabolic form [20]

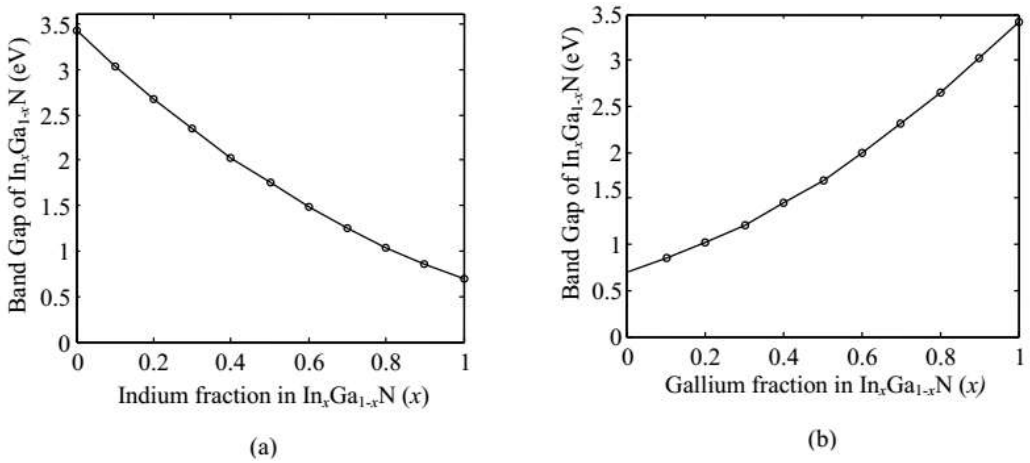

Fig-2: Composition of (a) In and (b) Ga in $In_xGa_{1-x}N$

$$E_{gInGaN}(x) = xE_{gInN} + (1-x)E_{gGaN} - bx(1-x). \quad (1)$$

Here E_{gInN} = 0.69 eV, E_{gGaN} = 3.4 eV, and the Bowing parameter, b=1.23 eV (for $In_xGa_{1-x}N$) [21]. Figure 2 shows the fraction of In and Ga in $In_xGa_{1-x}N$. For instance, as is shown in Fig. 2, for a given bandgap energy, the In fraction x in $In_xGa_{1-x}N$ can be calculated. To emit a laser output of 1.55 μm wavelength, E_g is 0.8 eV which corresponds to x = 0.15.

Lattice Constant

The chemical bonds of InGaN are predominantly covalent, which means that each atom is tetrahedrally bonded to four atoms of the other type. Because of the large difference in electro negativity of In and N atoms, there is a significant ionic contribution to the bond which determines the stability of the respective structural phase.

The lattice constants of the unstrained InGaN layer depend linearly upon the indium composition. Lattice constants a(x) and c(x) of $In_xGa_{1-x}N$ are predicted by Vegard's law as

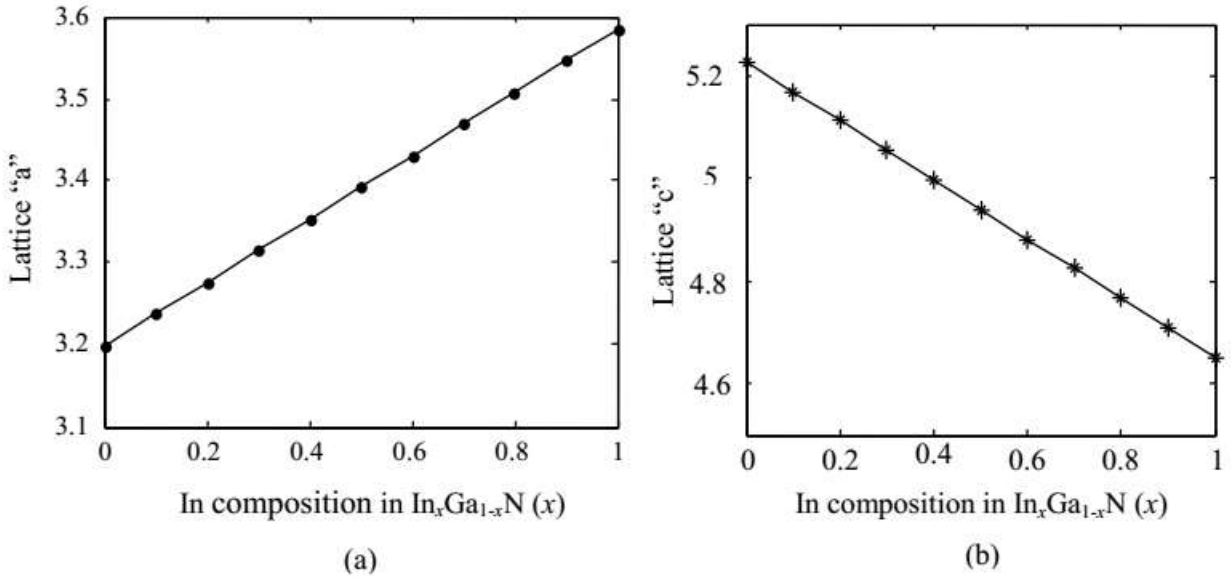

Fig-3: (a) Lattice constant a(x) of $In_xGa_{1-x}N$ and (b) Lattice constant c(x) of $In_xGa_{1-x}N$

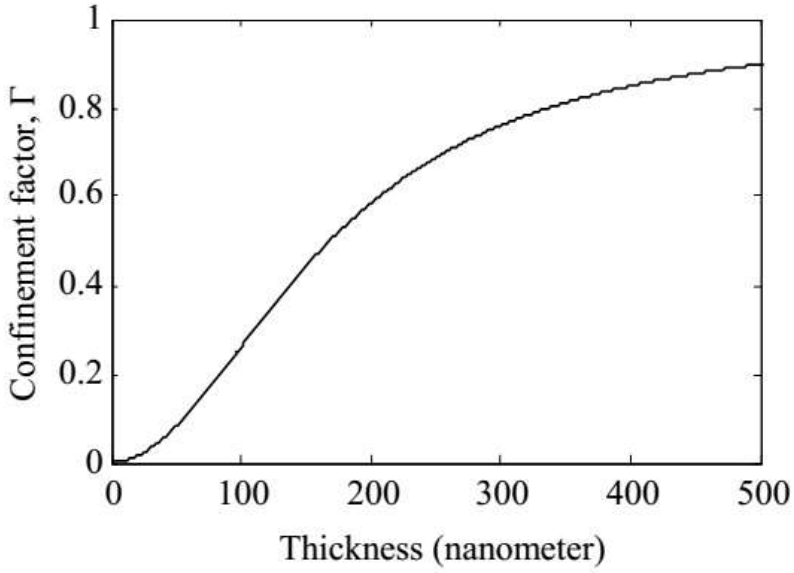

Fig-4: Active layer thickness vs. optical confinement factor

$$a_{InGaN}(x) = (3.1986 + 0.3862x)\,\text{Å}, \quad (2)$$

$$c_{InGaN}(x) = (5.2262 - 0.574x)\,\text{Å}. \quad (3)$$

For a given In composition of x = 0.15, as it is shown in Fig. 3, these two lattice constants a(x) and b(x) are calculated to be 3.2565 and 5.1401, respectively.

Optical Confinement Factor

Optical confinement factor is the ratio of the intensity of the light existing in the relevant layer to the total light intensity.

$$\Gamma^8 = 2\pi^2\left(n_a^2 - n_c^2\right)\left(\frac{d}{\lambda}\right)^2, \quad (4)$$

where $\Gamma = \dfrac{\Gamma^*}{1+\Gamma^8}$, n_a = Refractive index of the active layer, n_c = Refractive index of cladding layer and d is the active layer thickness.

Figure 4 shows that the optical confinement factor varies with active layer thickness. To design the proposed system model, an active layer thickness of 100 nm has been chosen. As is shown in the figure, the optical confinement factor is 0.24 corresponding to this thickness. The optical confinement factor Γ is an important parameter to design the optical losses or the optical gains in the optical waveguides.

Electronic Energy Bands

The ternary nitride compounds AlGaN and InGaN can be grown both as hexagonal as well as in cubic structures [22]. Growth of Cubic InGaN quantum wells with high structural and optical quality has been reported in Ref. [23]. To make the calculation simple we assumed a cubic structure for the proposed InGaN based laser.

The time independent Schrödinger equation is given by [24-25]

$$E(k_t = 0)\psi_i = \left[-\frac{\hbar^2}{2m^*}\nabla^2\psi_i + U_i\psi_i\right], \quad (5)$$

where $\nabla^2 = \dfrac{\partial^2}{\partial x^2} + \dfrac{\partial^2}{\partial y^2} + \dfrac{\partial^2}{\partial z^2}$.

The Poisson's equation in the semiconductor is written as [24]

$$\nabla \cdot (\varepsilon \nabla \Phi) = -\rho, \qquad (6)$$

where Φ is the electrostatic potential and ρ is the charge density, and are defined as $\rho = e(p - n + C_0)$ and $C_0 = N_D^+ - N_A^-$; where e = 1.6 x10^{-19} C is the magnitude of a unit charge, p is the hole concentration, n is the electron concentration, N_D^+ the ionized donor concentration, and N_A^- is the ionized acceptor concentration.

For one dimensional case (z-axis),

$$E\psi_i = \left[-\frac{\hbar^2}{2m^*}\frac{d^2}{dz^2} + U_i(z) \right] \psi_i(z). \qquad (7)$$

The energy dispersion relation for a single band n near k_0, (assuming 0) is given by [24]

$$E_n(k) = E_n(0) + \sum_{\alpha,\beta} \frac{\hbar^2}{2}\left(\frac{1}{m^*}\right)_{\alpha\beta} k_\alpha k_\beta. \qquad (8)$$

For the Hamiltonian H, with a periodic potential U(z) H_{op} is given by [24]

$$H_{op} \equiv \frac{\hbar^2}{2m}\frac{d^2}{dz^2} + U(z). \qquad (9)$$

(i) Conduction Band

In the InGaN quantum well, the conduction bands are assumed to be parabolic. The effective mass theory for the conduction band is obtained from the dispersion relation [24]

$$E(k) = \frac{\hbar^2 k^2}{2m^*}, \qquad (10)$$

where the effective-mass of the electron in the conduction band is $m^* = m_b^*$ in the barrier region and $m^* = m_w^*$ in the quantum well and in the presence of the quantum-well potential,

$$V(z) = \begin{cases} V_0 (= \Delta E_c) & |z| > \frac{L_w}{2} \\ 0 & |z| \le \frac{L_w}{2}, \end{cases} \qquad (11)$$

where the energies are all measured from the conduction band edge. For one dimensional case the time independent Schrödinger equation is given by [24]

$$E\psi_i = \left[-\frac{\hbar^2}{2m_e}\frac{d^2}{dz^2} + U_i(z) \right] \psi_i(z) \equiv \left[H_{op} \right] \{\Psi\}. \qquad (12)$$

In this case the Hamiltonian operator is

$$H_{op} = \left[-\frac{\hbar^2}{2m_e}\frac{d^2}{dz^2} + U_i(z) \right]. \qquad (13)$$

In finite difference [25] technique,

$$\left(\frac{\partial \Psi^2}{\partial z^2}\right)_{z=z_n} \rightarrow \frac{1}{a^2}\left[\Psi_{i+1}(z) - 2\Psi_i(z) + \Psi_{i-1}(z)\right] \text{ and } U(z)\Psi(z) \rightarrow U(z_n)\Psi(z_n).$$

Let $t_0 = \frac{\hbar^2}{2m_e a^2}$. This allows us to write, $\left[-\frac{\hbar^2}{2m_e}\frac{d^2}{dz^2} + U_i(z) \right] \Psi_i(z)$

$$= -\frac{\hbar^2}{2m_e a^2}\left[\Psi_{i+1}(z) - 2\Psi_i(z) + \Psi_{i-1}(z)\right] + U_i(z)\Psi_i(z) = (U_i(z) + 2t_0)\Psi_i(z) - t_0\Psi_{i-1}(z) - t_0\Psi_{i+1}(z).$$

So the 4x4 Hamiltonian matrix becomes

$$H = \begin{bmatrix} 2t_0 + U_1 & -t_0 & 0 & 0 \\ -t_0 & 2t_0 + U_2 & -t_0 & 0 \\ 0 & t_0 & 2t_0 + U_3 & -t_0 \\ 0 & 0 & -t_0 & 2t_0 + U_4 \end{bmatrix}.$$

Now the time independent Schrödinger equation can be written as

$$E \begin{Bmatrix} \Psi_1 \\ \Psi_2 \\ \Psi_3 \\ . \\ . \\ \Psi_{N-1} \\ \Psi_N \end{Bmatrix} = \begin{bmatrix} 2t_0 + U_1 & -t_0 & 0 & 0 & . & 0 \\ -t_0 & 2t_0 + U_2 & -t_0 & 0 & . & 0 \\ 0 & -t_0 & 2t_0 + U_3 & -t_0 & . & 0 \\ . & . & . & . & . & . \\ . & . & . & . & . & . \\ 0 & 0 & . & . & 2t_0 + U_{N-1} & -t_0 \\ 0 & 0 & 0 & 0 & -t_0 & 2t_0 + U_N \end{bmatrix} \begin{bmatrix} \Psi_1 \\ \Psi_2 \\ \Psi_3 \\ . \\ . \\ \Psi_{N-1} \\ \Psi_N \end{bmatrix}.$$

The eigen-values and eigen-vectors of the Hamiltonian matrix give the corresponding conduction band energies and corresponding wave vectors [25] i.e. [V,D] = eig(H). Now the electron density in the conduction band is calculted from the wave functions Ψ, as the square of the wave function Ψ^2, represents electron density at any given point. Since the square of any real number is zero or positive, it is clear that electron density cannot be negative, as expected intuitively.

(ii) Valence Band

In the InGaN quantum well the valence bands are assumed to be non-parabolic. In this time the quantum-well potential is given by

$$V_h(z) = \begin{cases} 0 & |z| \le \frac{L_w}{2} \\ -\Delta E_c & |z| > \frac{L_w}{2}. \end{cases} \qquad (14)$$

The Luttinger-Kohn Hamiltonian matrix when depends on the wave function is defined as [20-21]

$$H^{LK} = \begin{bmatrix} P+Q & -S & R & 0 \\ -S^* & P-Q & 0 & R \\ R^* & 0 & P-Q & S \\ 0 & R^* & S^* & P+Q \end{bmatrix}, \qquad (15)$$

where the values of P, Q, R and S are given by [26]. $P = \frac{\hbar^2 \gamma_1}{2m_0}\left(k_t^2 + k_1^2 + \frac{\partial^2}{\partial z^2}\right)$,

$Q = \frac{\hbar^2 \gamma_2}{2m_0}\left(k_t^2 + k_1^2 - 2\frac{\partial^2}{\partial z^2}\right)$, $R = \frac{\sqrt{3}\hbar^2}{2m_0}\left[-\gamma_2\left(k_t^2 - k_2^2\right) + 2i\gamma_3 k_1 k_2\right]$ and

$S = \frac{\hbar^2 \gamma_3}{m_0}\sqrt{3}\left(k_t - ik_2\right)\frac{\partial}{\partial z}$.

Now,

$$P + Q = \frac{\hbar^2}{2m_0}\left[\left(\gamma_1 + \gamma_2\right)k_t^2 - \left(\gamma_1 - 2\gamma_2\right)\frac{\partial^2}{\partial z^2}\right],$$

$$P - Q = \frac{\hbar^2}{2m_0}\left[\left(\gamma_1 - \gamma_2\right)k_t^2 - \left(\gamma_1 + 2\gamma_2\right)\frac{\partial^2}{\partial z^2}\right].$$

For Luttinger-Kohn Hamiltonian matrix, $E\Psi_{hi} = H\Psi_{hi}(z)$.

Taking $t_0 = \frac{\hbar^2}{2m_e a^2}$, and using the finite difference method [18], one can get

$$(P+Q)\Psi_{j,n}(z) = \left\{\frac{\hbar^2}{2m_0}\left[(\gamma_1+\gamma_2)k_t^2 - (\gamma_1-2\gamma_2)\frac{\partial^2}{\partial z^2}\right] + U_i(z)\right\}\Psi_{j,n}(z)$$

$$= \left\{\frac{\hbar^2}{2m_0}\left[(\gamma_1+\gamma_2)k_t^2 - (\gamma_1-2\gamma_2)\frac{(-2)}{a^2}\right] + U_i(z_i)\right\}\Psi_{j,n}(z_i) +$$

$$\left\{\frac{\hbar^2}{2m_0}\left[(\gamma_1+\gamma_2)k_t^2 - (\gamma_1-2\gamma_2)\frac{1}{a^2}\right] + U_{i-1}(z_{i-1})\right\}\Psi_{j,n}(z_{i-1})$$

$$= A_i\Psi_{j,n}(z_i) + B_i\Psi_{j,n}(z_{i+1}) + B_i\Psi_{j,n}(z_{i-1}). \qquad (16)$$

Where

$$A_i = \frac{\hbar^2}{2m_0}\left[(\gamma_1+\gamma_2)k_t^2 - (\gamma_1-2\gamma_2)\frac{(-2)}{a^2}\right] + U_i(z_i),$$

$$B_i = \frac{\hbar^2}{2m_0}\left[(\gamma_1+\gamma_2)k_t^2 - (\gamma_1-2\gamma_2)\frac{1}{a^2}\right] + U_{i-1}(z_{i-1}).$$

Similarly,

$$(P-Q)\Psi_{j,n}(z) = A_i'\Psi_{j,n}(z_i) + B_i'\Psi_{j,n}(z_{i+1}) + B_i'\Psi_{j,n}(z_{i-1}),\ (-S)\Psi_{j,n}(z) = -\frac{\sqrt{3}\hbar^2\gamma_3}{m_0}(k_t - ik_2)\frac{\partial}{\partial z}\Psi_{j,n}(z)$$

$$= -\frac{\sqrt{3}\hbar^2\gamma_3}{m_0}(k_t - ik_2)\frac{\Psi_{j,n}(z_{i+1}) + \Psi_{j,n}(z_{i-1})}{2a}$$

$$= C_i\Psi_{j,n}(z_{i+1}) + C\Psi_{j,n}(z_{i-1}). \qquad (17)$$

Where $C_i = -\frac{\sqrt{3}\hbar^2\gamma_3}{m_0}(k_t - ik_2)\frac{1}{2a}$, $R\Psi_{j,n}(z_i) = \frac{\sqrt{3}\hbar^2}{2m_0}\left[-\gamma_2(k_t^2 - k_2^2) + 2i\gamma_3 k_1 k_2\right]\Psi_{j,n}(z_i)$.

RESULT AND DISCUSSION

We have calculated the subband energies for the conduction band (Cl) and the valence bands (HH and LH) as a function of the InGaN well width. In the whole work, the effect of lattice mismatch and strain were not considered. In the InGaN quantum well, the conduction bands are assumed to be parabolic and the valence bands to be non-parabolic. These bands have been computed by solving the Schrödinger equation using **k.p** method with a 4×4 Luttinger-Kohn Hamiltonian matrix operator. The physical parameters that have been used for simulations are listed in Table 1. These parameters such as binary effective mass, lattice constants, elastic constants are linearly interpolated to obtain InGaN values from InN and GaN values using the following formula [16]

Table-1: The values of the parameters of InN and GaN used in the simulation model

Parameter	Symbol	Unit	InN	GaN	Refs.
Electron effective mass	m^*	m_0	0.11	0.20	[27]
Hole effective mass parameter	A_1 A_2 A_3 A_4	—	-9.24 -0.60 8.68 -4.34	-7.24 -0.51 6.73 -3.36	[27]
Lattice constants	a c	Å Å	3.548 5.751	3.182 5.173	[28]
Luttinger parameter	γ_1 γ_2 γ_3		3.72 1.26 1.63	2.70 0.76 1.07	[29]
Electron affinity	χ	eV	5.8	4.1	[30]
Thermal conductivity		(W/cmK)	0.45	1.3	[31]
Dielectric constant			15.3	8.9	[31]

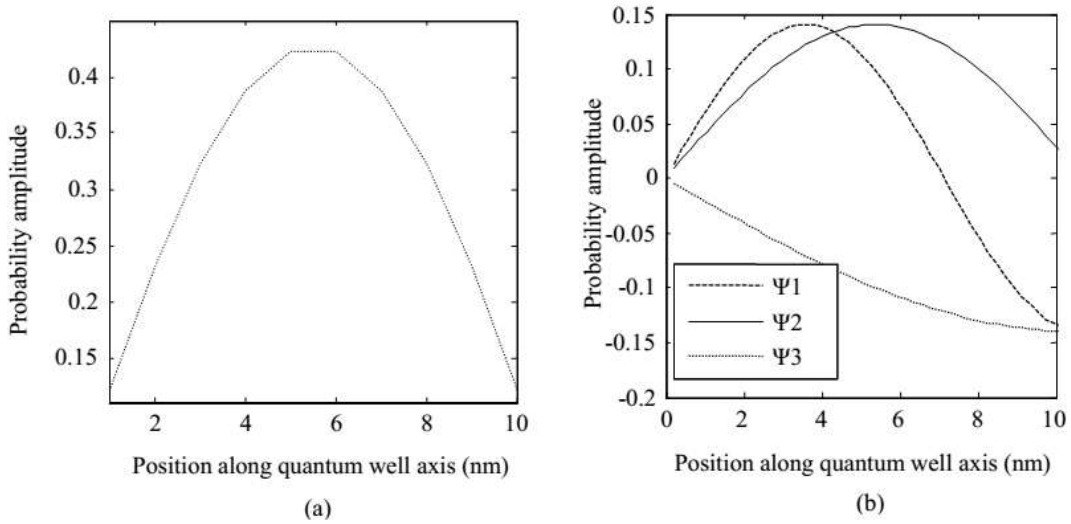

Fig-5: (a) Probability distribution corresponding to the lowest eigen value and (b) Probability distribution corresponding to the three eigen values.

$$P(In_xGa_{1-x}N) = xP(InN) + (1-x)P(GaN) \cdot$$

In the analysis of QW structures using the **k.p** method for the calculation of the electronic band dispersion, a confining potential V(*z*) along the growth direction *z* is added and k becomes an operator in the **k.p** Hamiltonian.

The radial probability distribution (i.e. finding the electron in an orbital at any given distance away from the nucleus) explicitly gives the probability of finding the electron in the volume of the quantum well of the laser. The probability distributions corresponding to the eigen values of the Hamiltonian of the time independent one dimensional Schrödinger equation for conduction subbands only are shown in Fig. 5. Figure 6(a) illustrates the electron density in the quantum well corresponding to the probability distribution mentioned in Fig. 5. The maximum electron density is found to be 10^{18} cm^{-3} and is shown in Fig. 6(a). The calculated conduction band dispersion profile is shown in Fig. 6(b). Apart from the band edge ($k_t = 0$), the energy is found to increase gradually with wave vector.

The valence band, heavy holes and light holes of InGaN based quantum wells have been considered in order to explain the mixing between the valence band states. For the valence band states, the upper four states have been explicitly treated [29] in InGaN QW structure, because they are very close to one another due to the small spin-orbit and crystal-field splitting energies. In Fig. 7 HH1, HH2, and HH3 indicate the first, second, and third heavy holes and LH1 is the first light hole. For any well length, the coupling between HH bands and the other kinds of bands is weak; hence the HH bands are nearly parabolic. The energies of the electron for the heavy-hole and light-hole subbands (see Fig. 7) are plotted as a function of the wave number. It is seen that the magnitudes of all energy levels decrease with the increase of wave number. It is found that the band mixing effect between heavy and light holes is less for our InGaN based lasers. These results are in good agreement with the findings presented by Piprek et al. [27].

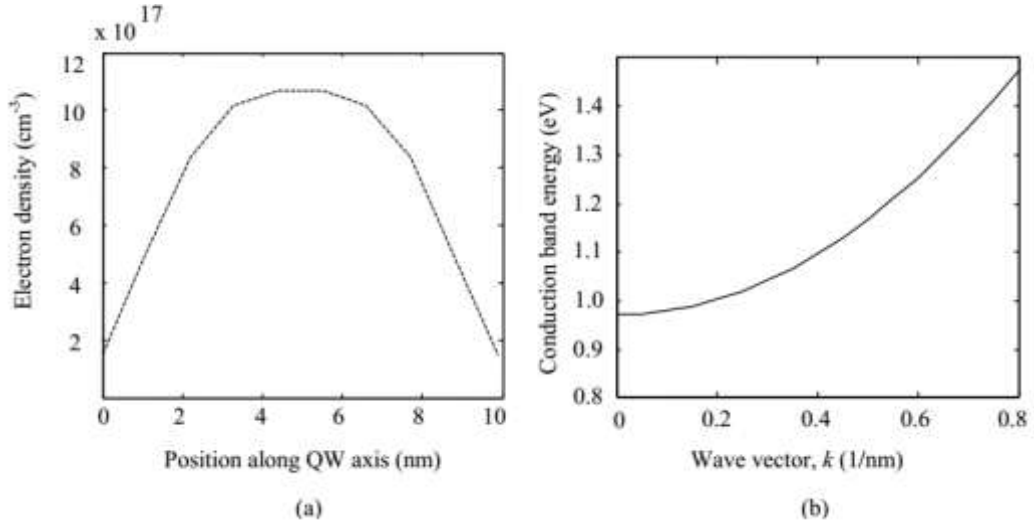

Fig-6: (a) Electron density profile in conduction band and (b) Energy of the first conduction subband (C1).

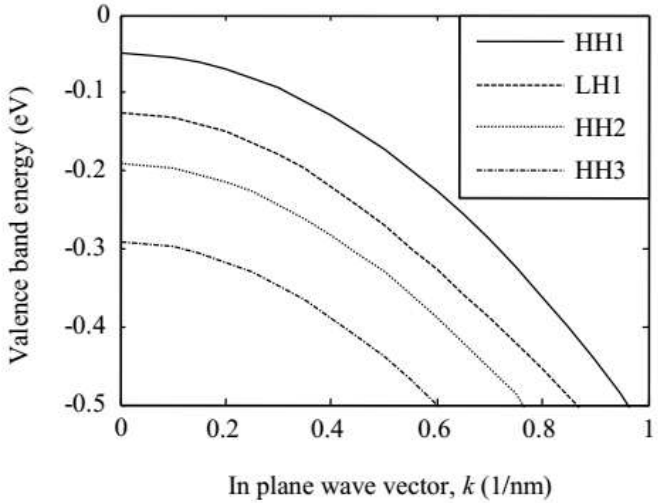

Fig-7: The valence subband dispersion functions of the first conduction and heavy hole bands of quantum well

CONCLUSION

In this paper, the physical properties of the proposed InGaN based heterostructure quantum well lasers were studied briefly. The required In composition for 1.55 μm wavelength and lattice constants were determined first. An In composition of 15% is required for the laser emission of this wavelength. Later, the physical length was demonstrated so that light can confine in the structure. A 100 nm active layer thickness is found to be enough to sufficiently confine the laser light. In addition, the band profiles were also demonstrated to calculate the carrier density and to mapping the mixing among bands. A carrier electron density of 10-18 cm-3 was the result of the investigation. The findings are in well agreement with the previously reported results of other structures.

REFERENCES

1. Yu, S., Luo, M., Li, X., Hu, R., Qiu, Y., Li, C., Liu, W., He, Z., Zeng, T., & Yang, Q. (2016). Recent progress in an 'ultra-high speed, ultra-large capacity, ultra-long distance' optical transmission system (Invited Paper). Chinese Optics Letters, 14, 120003.
2. Bae, S. H., Kim, H., & Chung, Y. C. (2016). Transmission of 51.56-Gb/s OOK signal using 1.55-μm directly modulated laser and duobinary electrical equalizer. Optical Express, 24, 22555-22562.
3. Ackert, J. J., Thomson, D. J., Shen, L., Peacock, A. C., Jessop, P. E., Reed, G. T., Mashanovich, G. Z., & and Knight, A. P. (2015). High-speed detection at two micrometres with monolithic silicon photodiodes. Nature Photonics, 9, 393–396.
4. Heck, M. J. R. (2008). Ultrafast integrated semiconductor laser technology at 1.55 μm, Eindhoven: Technische Universiteit Eindhoven.
5. Korpijärvi, V. -M. et al. (2014). 1.55 μm GaInNAsSb/GaAs Ridge Waveguide Lasers and Semiconductor

Optical Amplifiers for Photonic Integrated Circuits. Proc. International Semiconductor Laser Conference, Palma de Mallorca, 151-152.
6. Otsubo, K. *et al*., (2009). 1.3-μm AlGaInAs Multiple-Quantum-Well Semi-insulating Buried-Heterostructure Distributed-Feedback Lasers for High-Speed Direct Modulation. *IEEE Journal of Selected Topics in Quantum Electronics*, 15(3), 687-693.
7. Michalzik, R. (2013). Fundamentals, Technology and Applications of Vertical-Cavity Surface-Emitting Lasers, Springer-Verlag Berlin Heidelberg.
8. Okamoto, K., Ohta, H., Chichibu, S. F., Ichihara, J., & Takasu, H. (2007). Continuous-Wave Operation of m-Plane InGaN Multiple Quantum Well Laser Diodes. Japanese Journal of Applied Physics, 46(2), 8–11.
9. Rafailov, E. U., Cataluna, M. A. & Sibbett, W. (2007). Mode-locked quantum-dot lasers. Nature Photonics, 1, 395 – 401.
10. Loehr, P. J., & Sing, J. (1991). Theoretical Studies of the Effect of Strain on Performance of Strained Quantum Well Lasers Based on GaAs and InP Technology. IEEE Journal of Quantum Electron, 27(3), 708–716.
11. Goddard, L. L., Bank, R. S., Wistey, A. M., Tuen, B. H., Zhilong, R., & Harris, S. J. (2005). Recombination, gain, band structure, efficiency, and reliability of 1.5μm GaInNAsSb/GaAs lasers. Journal of Applied Physics, 97, 083101-083101-15.
12. Goddard, L. L., Bank, R. S., Wistey, A. M., Tuen, B. H., Zhilong, R., & Harris, S. J. (2005).High-performance GaInNAsSb/GaAs lasers at 1.5μm. Proc. SPIE-Photonics West 2005, 5738, 180-191.
13. Sarzala, R. P., & Nakwaski, W. (2007). GaInNAsSb/GaNAs quantum-well VCSELs: Modeling and physical analysis in the 1.50-1.55 μm wavelength range. Journal of Applied Physics, 101, 073103 - 073103-7.
14. Park, S. W. (1997). Threshold Current Density and Differential Gain in InGaAs/InGaAlAs Strained Quantum Well Lasers. Journal of the Korean Physical Society, 30, 280-285.
15. Hasan, M. T., Islam, M. J., Hasan, R. –U., Islam, M. S., Yeasmin, S., Bhuiyan, A. G.., Islam, M. R., & Yamamoto, A. (2010). Design and performance of 1.55 μm laser using InGaN. Physica Status Solidi C, 7, 1825-1828.
16. Smowto, P. M. et al. (2002). The Effect of Cladding Layer Thickness on Large Optical Cavity 650-nm Lasers. IEEE Journal of Quantum Electronics, 38(3), 285-290.
17. Nakamura, S. et al. (1997). Room-temperature continuous-wave operation of InGaN multi-quantum-well structure laser diodes with a lifetime of 27 hours. Applied Physics Letters, 70(1), 1417-20.
18. Davydov, V. Y. et al. (2002). Rapid Research Note Band Gap of InN and In-Rich InxGa1-xN alloys. Physica Status Solidi B, 230(2).
19. Xiao, H. et al. (2006). Research on the band-gap of InN grown on silicon substrates. Physica Status Solidi C, 3(3), 594 – 597.
20. Thahab, S. M., Hassan, H. A., & Hassan, Z. (2007). Performance and optical characteristic of InGaN MQWs laser diodes. Optics Express, 2380, 2380-2390.
21. Mukai, T., Yamada, M., & Nakamura, S. (1999). Characteristics of InGaN-Based UV/Blue/Green/ Amber/Red Light-Emitting Diodes. Japanese Journal of Applied Physics, 38, 3976–3981.
22. Lemos, V., Silveira, E., Leite, J. R., Tabata, A., & Trentin, R. (2000). Evidence for phase-separated quantum dots in cubic InGaN layers from resonant raman scattering. Physical Review Letters, 84(16), 3666–3669.
23. Berrah, S., Boukortt, A., & Abid, H. (2008). The composition effect on the bowing parameter in the cubic InGaN, AlGaN and AlInN alloys. Semiconductor Physics, Quantum Electronics & Optoelectronics, 11(1), 59-62.
24. Lien Chuang, S. (2008). Physics of Optoelectronic Devices, (2nd ed.). Wiley-Interscience publication.
25. Datta, S. (2005). Quantum Transport: Atom to Transistor, (2nd ed.). New York, Cambridge University Press.
26. Singh, J. (2003). qwkpvb-Quantum Well k.p Valence Subband Software USER'S MANUAL. Department of Electrical Engineering and Computer Science, University of Michigan, Ann Arbor, Michigan.
27. Piprek, J., & Nakamura, S. (2002). Physics of high-power InGaN/GaN lasers. IEE Proceedings of Optoelectronics, 149(4), 145 – 151.
28. Yan, Q., Rinke, P., Winkelnkemper, M., Qteish, A., Bimberg, D., Scheffler, M., & Van deWalle, C. G. (2011). Band parameters and strain effects in ZnO and group-III nitrides. Semiconductor Science and Technology, 26(1), 1-8.
29. Nakamura, S., & Chichibu, S. F. (2000). Introduction to Nitride Semiconductor Blue Lasers and Light Emitting Diodes, New York , CRC Press.
30. Krukowski, S., Witek, A., Adamczyk, J., Jun, J., Bockowski, M., Grezegory, I., & Zinn (1998). Thermal properties of Indium Nitride. Journal of Physics and Chemistry of Solids, 59(3), 289-295.
31. Park, S. -H. (2008). Optical Gain of Type-II 1.55-μm GaAsSb/InGaNAs/GaAs Trilayer Quantum Wells. Journal of the Korean Physical Society, 53(4), 1886-1890.